

# Equilibrium analysis of steady state tokamak discharges

W. Zwingmann

Association Euratom-CEA/DSM/DRFC Cadarache 13108 St-Paul-Lez-Durance, France

Received 31 October 2002, accepted for publication 27 June 2003

Published 26 August 2003

Online at [stacks.iop.org/NF/43/842](http://stacks.iop.org/NF/43/842)

## Abstract

Equilibrium reconstruction is the essential diagnostic tool for determining the magnetic field and current density of a tokamak discharge. This method parametrizes the unknown current profile with a suitable set of test functions and determines the coefficients from measurements. For steady state discharges, a continuous equilibrium analysis is required. The purpose of the Tore Supra CIEL project is the study of discharges with duration up to 1000 s. We report on the development of a real-time version of the widely used equilibrium code EFIT.

**PACS numbers:** 52.55.Dy, 52.55.Fa, 28.52.Av

## 1. Introduction

The steady state operation of a tokamak discharge requires continuous monitoring and feedback of many discharge parameters. Accurate knowledge of the magnetic field structure and the current distribution in a tokamak is of fundamental importance for achieving optimum performance. However, it is very difficult to measure these quantities in fusion plasma directly. One therefore relies on the method of equilibrium reconstruction. This method uses data from magnetic measurements at the vessel and internal plasma data to determine the equilibrium using MHD. Due to the nonlinearity of the static MHD equation, this task has to be solved numerically (for a comprehensive review, see [1]).

The numerical algorithms are CPU intensive and difficult to achieve in real-time. An approach to obtain the full equilibrium solution in real-time is the function parametrization or neural network method [2]. These methods avoid the actual calculation by pre-computing a large database of equilibria with a very accurate predictive solver. The actual equilibrium is found by interpolating using the database. The quality of the reconstruction is therefore directly linked to the precision of the solver and the completeness of the database. Any features not provided during the training of the database, like a fine structure of the current profile, is therefore excluded from the solution space. Another obvious problem poses the accurate predictive modelling of the nonlinear behaviour of the ferromagnetic material in tokamaks with a transformer.

In contrast, the direct method calculates the equilibrium for each set of measurements individually by solving the static MHD equation. One parametrizes the unknown current profile with a suitable set of test functions and determines the free parameters by fitting to measurements. We will show that accurate modelling of the field far away from the plasma

is not necessary, unlike a predictive solver for the function parametrization method. Various codes have been developed [3–10]. One of the most widely used codes is EFIT [3,4], which is in routine use for many tokamaks, for example, DIII-D, JET, and Tore Supra. The EFIT algorithm has the potential for real-time application, which will be further exploited in this paper.

The accuracy of the direct reconstruction depends on measurements of variables effectively present in the equilibrium problem, which are magnetic field and total kinetic pressure for the static force balance. The most reliable and precise direct measurement, the magnetic field and poloidal flux, is only available outside the discharge. However, using this data alone is not sufficient to obtain the current profile accurately, because its extrapolation into the discharge is a mathematically ill-posed problem [7]. Errors of the input data are significantly amplified in the centre of the plasma, and especially quantities like the central safety factor can be quite inaccurate [11, 12]. To achieve a high accuracy of the reconstruction, one has to obtain direct measurements of total pressure or safety factor, or the magnetic field inside the discharge. The EFIT code is able to use data from the Faraday rotation, motional Stark effect (MSE), total kinetic pressure, safety factor, and the diamagnetic effect of the plasma. The kinetic pressure and the safety factor are not readily available and require careful pre-processing of experimental data. The Faraday rotation diagnostics [6], which is installed on the Tore Supra tokamak (figure 1), provides information about the magnetic field inside the plasma. It gives the polarization angle  $\alpha$  integrated over the line of sight

$$\alpha = D \int n_e \mathbf{B} \cdot d\mathbf{s}, \quad (1)$$

where  $D$  is an appropriate constant, and  $n_e$  the electron density. A local measurement of the field is given by measurement of

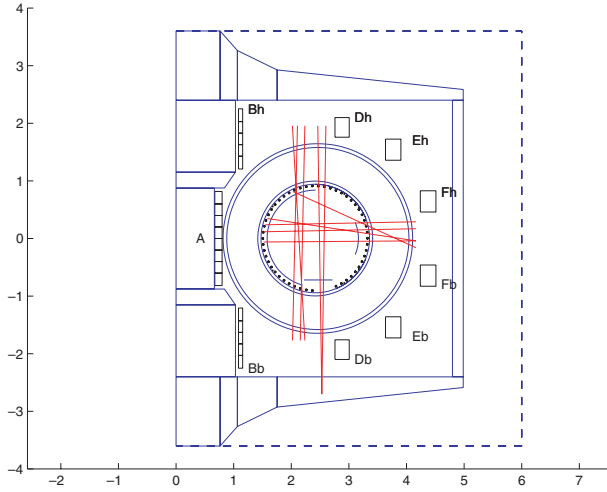


**Figure 1.** View of the tokamak Tore Supra showing the present CIEL configuration, with the iron transformer and the poloidal field system. The figure shows the real shape of the 6 transformer limbs (---), and their axisymmetric model used for field calculations. The axisymmetric model was chosen to preserve the radial cross section of the transformer limbs. The squares inside the vacuum vessel mark the position of the 52 tangential and 52 normal poloidal field coils and circles the 6 flux loops of the magnetic diagnostics. The figure shows the 10 viewing lines of the Faraday rotation diagnostics.

the motional Stark effect (MSE), which is present in neutral beam heated plasma due to the induced electric field  $\mathbf{E} = \mathbf{v}_{\text{NBI}} \times \mathbf{B}$ . It exploits the relation [13, 14]

$$\tan \gamma = \frac{E_R}{E_Z} = \frac{A_0 B_Z + A_1 B_R + A_2 B_T}{A_3 B_Z + A_4 B_R + A_5 B_T}, \quad (2)$$

where  $\gamma$  is the measured pitch angle, ( $B_R$ ,  $B_T$ ,  $B_Z$ ) the local magnetic field, and  $A_n$ ,  $n = 0, \dots, 5$  coefficients dependent on the viewing geometry.

We derive the algorithm of direct equilibrium reconstruction for a tokamak in the general case of anisotropic pressure, and in the presence of a ferromagnetic transformer. The approach presented in this paper is compared with other direct methods [7, 10]. The following section describes the model of the iron transformer and validates the model using a dry run with no plasma. We report on the optimized implementation of the reconstruction model and give results the accuracy of the reconstruction, and the CPU timing for the Tore Supra tokamak.

## 2. Direct equilibrium reconstruction

We allow for the more general case of anisotropic pressure, but neglect plasma flow. Assuming toroidal symmetry of the tokamak and the discharge, the poloidal flux  $\Psi(R, Z)$  is given by a Grad–Shafranov type equation [15, 16]. With the abbreviations

$$\Delta^* := \frac{\partial^2}{\partial R^2} - \frac{1}{R} \frac{\partial}{\partial R} + \frac{\partial^2}{\partial Z^2},$$

$$P'_{\parallel} := \frac{\partial P_{\parallel}(\Psi, R)}{\partial \Psi}, \quad FF' := F \frac{\partial F(\Psi)}{\partial \Psi},$$

one obtains

$$-\Delta^* \Psi = \mu_0 R J_{\text{tor}} = R^2 \mu_0 P'_{\parallel} + FF' + \mu_0 R J_{\text{ext}}. \quad (3)$$

$P'_{\parallel}$  and  $FF'$  are the two profiles describing the plasma current  $J_{\text{plasma}}$ , and  $J_{\text{ext}}$  denotes the current distribution of all external sources outside the plasma. The direct equilibrium reconstruction determines the unknown profiles  $P'_{\parallel}$  and  $FF'$ , and the source term  $J_{\text{ext}}$  for each time sample of measurement.

For the isotropic case,  $P_{\parallel}(\Psi, R)$  becomes  $P(\Psi)$ , such that the toroidal current depends only on the poloidal flux  $\Psi$ . In either case, the unknown current profile is parametrized as a linear superposition of suitable test functions with  $N_f$  unknown coefficients  $c_k$

$$J_{\text{plasma}}(\Psi, R) = \sum_{k=1}^{N_f} c_k J_k(\Psi, R). \quad (4)$$

The external sources are constituted by the currents in the poloidal field coils, induced currents in the vacuum vessel, support structures, limiter and blanket. In tokamaks with an iron-core transformer, like JET or Tore Supra, one has to consider the field produced by the induced magnetization in ferromagnetic materials. There are two approaches to treat external sources:

1. The finite domain approach selects a finite boundary around the plasma. Examples are the codes IDENTD [6] and equinox [10]. The poloidal flux at the domain boundary is provided by interpolation of magnetic measurements. Most present tokamaks provide the position of the plasma boundary in real-time using a suitable expansion of the vacuum region surrounding the plasma. These expansions give the poloidal flux in the vicinity of the magnetic sensors with sufficient accuracy. The finite domain code avoids modelling of the external sources and subsequent introduction of additional fitting variables other than those in the current profile (4). Current carrying structures between magnetic sensors and the plasma, like limiter structures or the blanket, are an exception.

One should note that in a finite domain code, experimental error cannot easily be attributed to the flux at the boundary. The solution domain has to be chosen close to the magnetic sensors, which rules out simple rectangular boundaries. Therefore, the finite element method has to be used for inverting the Grad–Shafranov operator. Due to its design, the finite domain code does not provide a redundant algorithm to compare with real-time boundary codes, and offers no predictive calculations.

2. The infinite domain approach chooses to model the outside sources  $J_{\text{ext}}$  with a suitable model. The field produced by the poloidal field coils is known. For air-core tokamaks, like DIII-D or ITER,  $J_{\text{ext}}$  is therefore quite well defined, and can simply be imposed in the Grad–Shafranov equation (3). The method is immediately usable without relying on a different code and provides therefore redundancy to real-time boundary codes. Furthermore, it allows for predictive modelling of discharges with the same code. Since there are no boundary conditions, a very fast solver can be used to solve the Grad–Shafranov equation.

The task of determining  $J_{\text{ext}}$  for a tokamak with an iron-core transformer, like JET or Tore Supra, is more difficult due to the induced magnetization in ferromagnetic materials, which is

inherently nonlinear. As shown below, accurate modelling of the field outside the plasma is not required. A suitable model has to be devised, introducing additional fitting parameters. The multipole model [5, 17] uses a linear superposition of Legendre functions [18]. The EFIT approach attempts to model external sources with their accurate geometry, including the iron transformer [21, 23].

We will now discuss in more detail the algorithm used in the code EFIT. The geometry of the external sources, such as the poloidal field coils, vacuum vessel, and the iron-core is well-known. The amplitude of the fields generated by vessel currents or magnetization is introduced as additional free parameter to be determined by the fitting procedure. In the EFIT approach for transformer tokamaks, the field from external sources is therefore split into a known part and a superposition of functions that reflect our knowledge of the geometry of the external sources with  $N_{\text{ext}}$  free parameters  $I_j$

$$\Psi_{\text{ext}}(R, Z) = \Psi_{\text{known}}(R, Z) + \sum_{j=1}^{N_{\text{ext}}} I_j \Psi_j(R, Z). \quad (5)$$

The model is also called Green's functions model and allows for calculation of the external flux contribution at any point in space. We define the vector of unknowns or state vector as  $\mathbf{x} := (I_j, c_k)^T$ , which is obtained by minimizing the least-squares functional

$$\chi^2 = \sum_{m=1}^{N_{\text{meas}}} \frac{1}{\sigma_m^2} (F_m^{\text{calc}}\{\Psi; \mathbf{x}\} - F_m^{\text{meas}})^2 + \lambda^2 \mathfrak{R}_{\text{plasma}} + \eta^2 \mathfrak{R}_{\text{ext}} \quad (6)$$

with the Grad-Shafranov type equation (3) as a constraint.  $F_m^{\text{meas}}$  is the measured value,  $\sigma_m$  is the estimated uncertainty of the measurement, and  $F_m^{\text{calc}}$  a functional to recalculate it from the flux function and the coefficients. Since the reconstruction problem is inherently ill-posed, one has to add a Tikhonov regularizing term [19]. The first term  $\lambda^2 \mathfrak{R}_{\text{plasma}}$  controls unwanted oscillations of the current profile  $J_{\text{plasma}}$  on a numerical scale of the test functions. A typical choice is

$$\mathfrak{R}_{\text{plasma}} = \int_{\Psi_{\text{axis}}}^{\Psi_{\text{boundary}}} \left( \frac{\partial^2 J_{\text{plasma}}}{\partial \Psi^2} \right)^2 d\Psi. \quad (7)$$

The choice of  $\lambda$  can strongly influence the results of the reconstruction. If  $\lambda$  is too small, the solution can develop oscillations, or the algorithm does not converge at all. If  $\lambda$  is too large, the solution is over-smoothed with loss of precision. We refer to an earlier paper [16] for an algorithm giving the correct choice of this parameter, applied to the reconstruction of an equilibrium with an inverted current profile. In a similar way, the term  $\eta^2 \mathfrak{R}_{\text{ext}}$  acts as a constraint on the external sources to avoid large amplitudes

$$\mathfrak{R}_{\text{ext}} = \sum_j (I_j - I_j^{\text{pred}})^2, \quad (8)$$

where  $I_j^{\text{pred}}$  are approximate values for  $I_j$ . Unlike the regularizing term acting on the current profile, the reconstruction is not very sensitive to the value of  $\eta$  for a wide range. Likewise,  $I_j^{\text{pred}}$  does not need to be specified accurately.

### 3. Validation of the iron transformer model

There have been several attempts to treat the iron transformer of a tokamak for reconstruction purposes (e.g. [20–23]). They are based on the representation with Green's functions (5), which is compatible with the EFIT approach. The field generated by the magnetization is related to the magnetization of the iron by

$$\mathbf{B}_{\text{iron}} = \nabla \times \mu_0 \left( - \oint \frac{\mathbf{n}' \times \mathbf{M}}{|\mathbf{x} - \mathbf{x}'|} da' + \int \frac{\nabla' \times \mathbf{M}}{|\mathbf{x} - \mathbf{x}'|} d^3x' \right) =: \mu_0 \hat{\Theta} \mathbf{M}. \quad (9)$$

The sections of the transformer are discretized into elements, and the magnetization assumed constant in each element. The relation (9) with the discretized integral operator  $\hat{\Theta}$  thus transforms into the desired superposition of test functions, and the magnetization of individual segments into the required fitting parameters. In principle, the representation (9) allows for the calculation of the magnetization in a self-consistent way. We observe that the total magnetic field is related to the magnetization through the permeability  $\mu(B)$  by  $\mathbf{B} = \mu \mu_0 \mathbf{M} / (\mu - 1)$ . The magnetization  $\mathbf{M}$  is then related to the applied field from poloidal field coils and plasma by the nonlinear algebraic equation

$$-\hat{\Theta} \mathbf{M} + \frac{\mu}{\mu - 1} \mathbf{M} = \frac{1}{\mu_0} (\mathbf{B}_{\text{plasma}} + \mathbf{B}_{\text{PFC}}). \quad (10)$$

Equation (10) forms the basis of the integral equation method [22, 24, 25]. However, the integral equation method leads to nonsparse matrices, which have to be inverted for each iteration cycle of a Newton scheme. An accurate solution of equation (10) requires too many variables, and is therefore not feasible for a fast reconstruction algorithm. On the other hand, it can be shown that only an approximate solution is required if one introduces the magnetization as first guess into the fitting term (8).

We define a closed surface  $\partial\Omega$  in the vicinity of the magnetic sensors surrounding the plasma. The fitting procedure then constrains the poloidal flux to be approximately

$$\Psi|_{\partial\Omega} \approx \Psi^{\text{plasma}}|_{\partial\Omega} + \Psi^{\text{ext}}|_{\partial\Omega}. \quad (11)$$

Since  $\Delta^* \Psi^{\text{ext}} = 0$  inside the domain,  $\Psi^{\text{ext}}$  is uniquely determined from its value at the boundary. The correct evaluation of the field outside the sensors, in particular at the iron transformer, is therefore not important. The EFIT approach gives correct results, if the fit to the magnetic gives small deviations within the accuracy of the measurement, and if there are enough degrees of freedom or enough variables for the external source model (5). The first condition, the good fit to measurements, is always monitored for the reconstruction. The second condition, the adequate size of the space of test functions, has to be verified by reconstructing a dry run without plasma, where only currents in the poloidal field coils are applied.

The relation (9) has been implemented for the Tore Supra tokamak. A further approximation is used by modelling the transformer limb using an axisymmetric model, shown in figure 1. The cross section in the axisymmetric model preserves the real cross section of the transformer limbs. The transformer section is subdivided into 14 segments,

giving 28 variables for vertical and radial coordinate of the magnetization. The iron model is validated with dry run 28571, exhibiting only currents in the poloidal field coils and no plasma. Figure 2(a) displays the currents applied, a constant Ohmic current of 3 kA, and currents in upper coils Bh, Dh, Eh and Fh applied in turn. The magnetization was obtained by minimizing the least-squares functional (6), setting the plasma components to zero.  $I^{\text{pred}}$  was obtained by solving equation (10), the regularization term (8) was used with  $\eta = 0.05$ . Figure 2(b) shows a typical time trace of a pick-up coil signal and its corresponding value calculated by the EFIT fitting procedure (6). Figure 2(c) gives the difference of all 102 measured signals versus the signals calculated by

EFIT. The deviation is of the order of 2 mT and thus below the error of measurement. This indicates that the iron model is able to reproduce a dry run with sufficient accuracy. The procedure was repeated for different values of  $\eta$  in the least-squares procedure (6). The reconstructed field of discharge 28571 at  $t = 65$  s is shown in figure 3. The figure compares the field for an optimal value of  $\eta = 0.05$  with an under-smoothed solution with  $\eta = 10^{-6}$ , and an over-smoothed solution with  $\eta = 10$ . Figure 3 shows that only over-smoothing the solution causes considerable deviation of the field structure. Over-smoothing is easily detected by an increase of the magnetic fitting error. Smaller values of the regularization may produce an unrealistic field outside the plasma, but never inside the

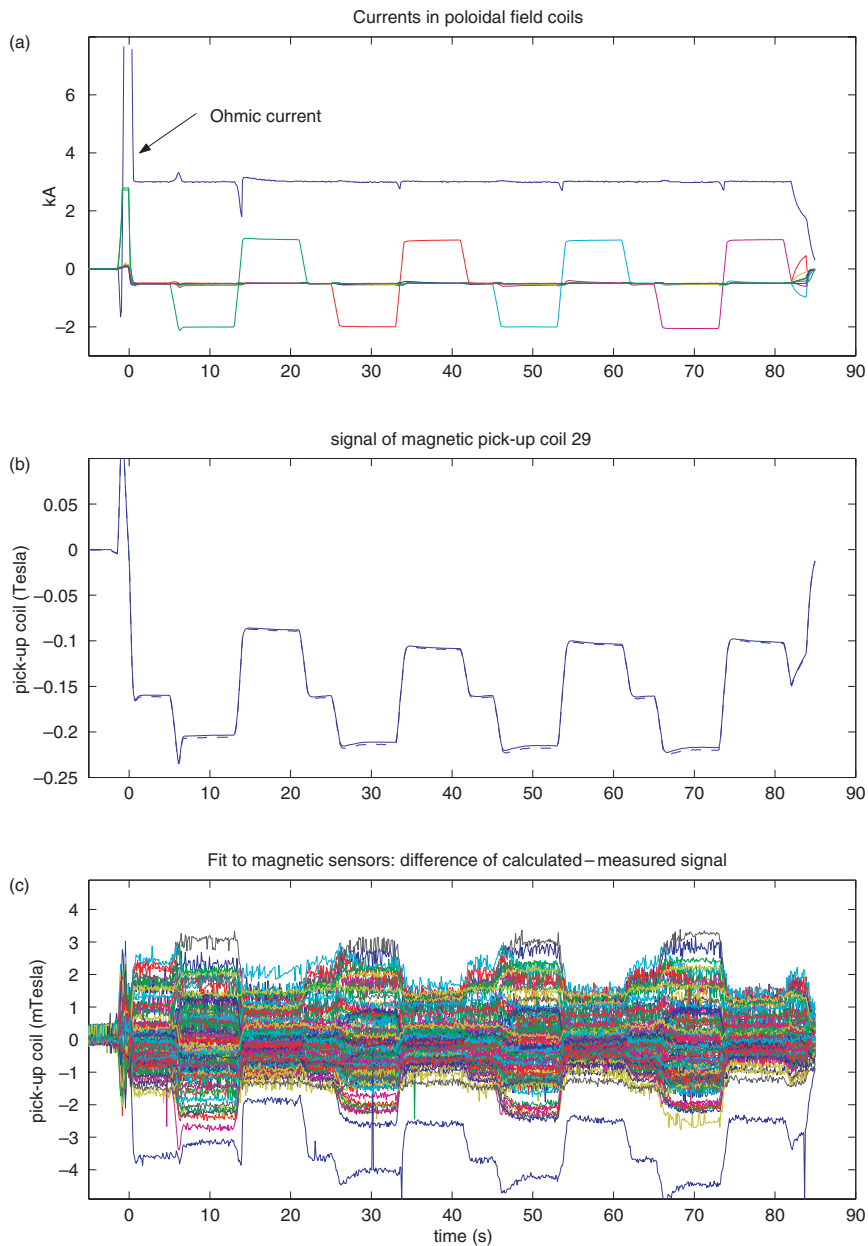


**Figure 2.** Validation of the iron model for Tore Supra dry run 28571. (a) shows the currents flowing in the poloidal field coils, with a constant Ohmic current of 3 kA. The remaining poloidal field coils are stimulated with a modulated current of  $-0.5$  kA. The square pulses are applied in upper coils Bh, Dh, Eh, and Fh (see figure 1). (b) shows a comparison of the measured signal of pick-up coil 29 (---) with the value obtained from the EFIT fitting procedure. (c) displays signal differences of all 102 magnetic sensors, with the vertical range in mTesla. The difference is formed between the calculated signal with the EFIT reconstruction and the corresponding measured signal.

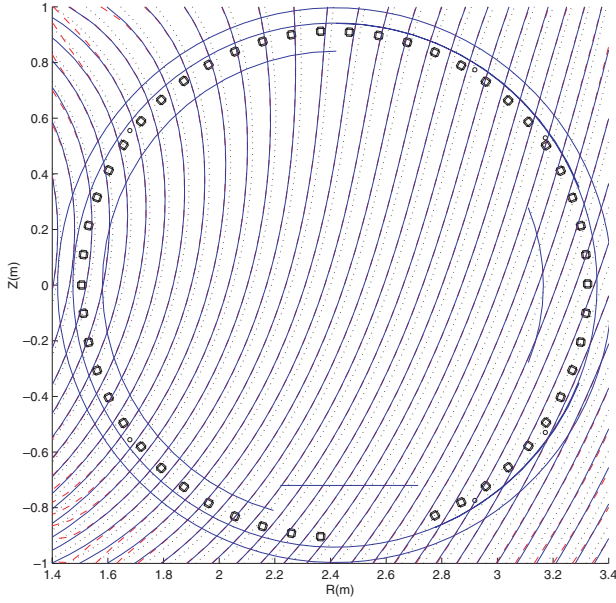


**Figure 3.** Reconstructed field configuration of dry run 28571 at  $t = 65$  s. This plot demonstrates the influence of the regularizing or smoothing parameter  $\eta$  for the external field model in the least-squares procedure (6). The solid lines show the solution for the optimal value of  $\eta = 0.05$ . The dashed lines give the under-smoothed solution with  $\eta = 10^{-6}$ . Note that the optimal and the under-smoothed solutions are almost identical in the region encircled by the magnetic sensors. The over-smoothed solution with  $\eta = 10$  ( $\dots$ ) shows considerable deviation, but is easily detected by an increase of the magnetic fitting error to  $\chi_{\text{mag}}^2 = 5$  from  $\chi_{\text{mag}}^2 = 2.7$  for the optimum solution.

domain encircled by the magnetic sensors. This supports the mathematical considerations given in the section above. The optimal value of  $\eta$  is therefore not very critical and is set to  $\eta = 0.05$  for the calculation of Tore Supra discharges.

#### 4. Implementation and optimization of the reconstruction algorithm

The reconstruction problem to determine the unknown current profile and external sources is nonlinear due to the Grad-Shafranov equation (3), and must therefore be solved iteratively. We apply the method of the Picard iteration. Given an initial flux distribution, the test functions  $J_k$  in equation (4) are calculated. The poloidal flux  $\Psi_k$  corresponding to  $J_k$  is calculated by inverting the Grad-Shafranov operator. This allows for calculating  $F_m^{\text{calc}}$  of the least-squares functional (6). Its minimization gives the updated vector of coefficients  $\mathbf{x}^{n+1}$ , the updated current density from equation (4), and the updated external field from equation (5). The iteration is repeated until convergence is achieved. Two individual steps of the algorithm have been identified as time-consuming, and we will discuss their effective implementation.

##### 4.1. Inversion of the Grad-Shafranov operator

The plasma contribution is obtained by inverting the Grad-Shafranov operator for all components of the current profile given by equation (4). The boundary condition for the poloidal

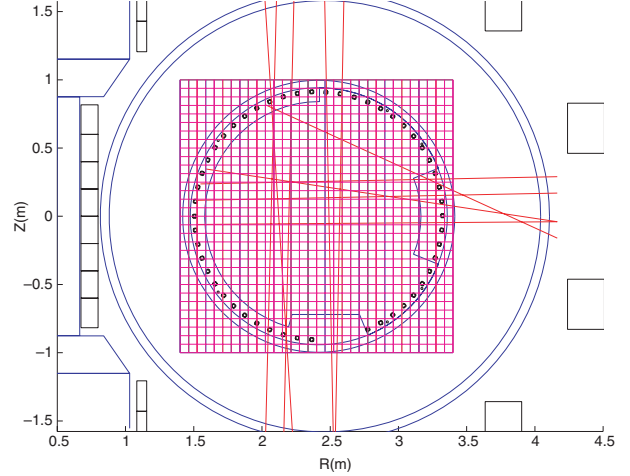


**Figure 4.** The rectangular grid used for the EFIT reconstruction with 33 radial and 33 vertical grid points.

flux is to vanish at infinity. We determine the solution of

$$\begin{aligned} -\Delta^* \Psi_k &= \mu_0 R J_k(R, Z), \\ \Psi_k|_{\infty} &= 0 \end{aligned} \quad (12)$$

with the very effective algorithm by Lackner [27], that introduces an artificial rectangular boundary outside the plasma and applies a rapid elliptic solver [1, 28]. The grid used for Tore Supra is shown in figure 4. It includes all measurements used for the plasma to allow for a fast interpolation at the sensor location. The CPU time for the algorithm is approximately  $t_1 N_g \log N_g + t_2 N_g$ , where  $N_g$  is the total number of grid points, and  $t_1$  and  $t_2$  are constants specific to the used computer. The Lackner algorithm is implemented in Fortran 95, using public domain libraries. Benchmarks are carried out on a 1 GHz MHz Compaq Alpha workstation with a speed of 1450 Linpack MFlops per processor. We achieve CPU times of 0.2 ms for a  $33 \times 33$  grid, and 4 ms for a  $129 \times 129$  grid.

##### 4.2. Compilation and minimization of the least-squares functional

The minimization of the least-squares functional (6) simplifies considerably for functionals  $F_m^{\text{calc}}$  that are linear in the poloidal field and therefore also in the state vector  $\mathbf{x}^{n+1} := (I_j, c_k)^T$  for iteration  $n+1$ . This is fulfilled for the magnetic diagnostic data, which measures poloidal flux differences or poloidal magnetic fields. Many internal plasma diagnostics data like Faraday rotation, MSE lead to a nonlinear term. In those cases, we linearize  $F_m^{\text{calc}}$  with respect to the strongest nonlinearity, the poloidal flux. We also request the Tikhonov regularizing term to be a quadratic form of the state vector. The weighted least-squares functional (6) is rewritten in standard form

$$\chi^2 = \|\mathbf{W} \cdot (\mathbf{A} \cdot \mathbf{x}^{n+1} - \mathbf{M})\|^2, \quad (13)$$

where the response matrix  $\mathbf{A}$  is defined by

$$\mathbf{A} := \begin{pmatrix} G^{\text{ext}} & G^{\text{plasma}} \\ C^{\text{ext}} & 0 \\ 0 & C^{\text{plasma}} \end{pmatrix}, \quad (14)$$

$G^{\text{plasma}}$  relates the measurement to the plasma current, and  $G^{\text{ext}}$  to the external sources.  $C^{\text{plasma}}$  and  $C^{\text{ext}}$  are the matrices corresponding to the regularizing terms. The least-squares measurement vector  $\mathbf{M}$  and the weight vector  $\mathbf{W}$  are defined as

$$\mathbf{M} := \begin{pmatrix} F^{\text{meas}} \\ 0 \\ 0 \end{pmatrix}, \quad \mathbf{W} := \begin{pmatrix} \left(\frac{1}{\sigma_m}\right) \\ \lambda \\ \eta \end{pmatrix}. \quad (15)$$

The linear least-squares problem (13) is solved with the procedure DGELS from the linear algebra library LAPACK [29], using the QR decomposition of  $\mathbf{W} \cdot \mathbf{A}$ .

The term  $G^{\text{plasma}}$  has to be calculated for each iteration step, because it depends on the flux function from the preceding iteration step. In the original EFIT algorithm,  $G^{\text{plasma}}$  was obtained by numerical integration for each measurement with the Biot–Savart law [9]. The operation count for this procedure scales with  $N_f * N_{\text{meas}} * N_g$  and leads therefore to unfavourable CPU times. Because the EFIT grid covers all sensors, we replace this integration with an interpolation on the  $\Psi_k$ , which we calculate with the rapid elliptic solver (12). One applies bicubic interpolation (e.g. [19]) that uses only the 16 adjacent grid values. Flux or field evaluation at a set of points  $\mathbf{r}^m$  can then be cast into a sparse matrix  $\mathbf{T}(\mathbf{L}, \mathbf{r}^m)$  acting on the column vector of flux at grid points  $\Psi$

$$\mathbf{L}\Psi(\mathbf{r}^m) \rightarrow \mathbf{T}(\mathbf{L}, \mathbf{r}^m)\Psi, \quad (16)$$

where  $\mathbf{L}$  is an arbitrary linear differential operator. Since the measurement points are fixed during the discharge, the matrices  $\mathbf{T}(\mathbf{L}, \mathbf{r}^m)$  can be pre-calculated. The operation count does no longer depend on the grid size, but scales with  $N_f * N_{\text{meas}}$  and is usually negligible. We illustrate the actual layout of  $G^{\text{plasma}}$  by the application to several individual measurements. The section of  $G^{\text{plasma}}$  covering the flux measurements is written as

$$G^{\text{flux}} = \mathbf{T}(\mathbf{1}, \mathbf{r}^{\text{flux}}) \cdot (\Psi_k), \quad (17)$$

where the columns of  $(\Psi_k)$  denote the discretized vector of poloidal flux at grid points, obtained by solving (12). The matrix corresponding to poloidal field measurements by pick-up coils is given by

$$G^{B_p} = \mathbf{T}\left(\frac{\mathbf{e}_T \times \mathbf{t}^{B_p}}{R^{B_p}} \cdot \nabla, \mathbf{r}^{B_p}\right) \cdot (\Psi_k), \quad (18)$$

$\mathbf{t}^{B_p}$  being the unit vector along the axis of a pick-up coil, and  $\mathbf{e}_T$  the unit vector in toroidal direction. The integral for evaluating the Faraday rotation (1) is discretized to give a summation over integration points  $\mathbf{r}^{\text{far}}$  with weights  $\mathbf{w}^{\text{far}}$  and unit vector  $\mathbf{t}^{\text{far}}$  along the viewing line, such that we arrive at

$$G^{\text{Faraday}} = \left( D \sum_{\text{Far}} \mathbf{w}^{\text{far}} n_e(\Psi^n(\mathbf{r}^{\text{far}})) \right) \times \mathbf{T}\left(\frac{\mathbf{e}_T \times \mathbf{t}^{\text{far}}}{R^{\text{far}}} \cdot \nabla, \mathbf{r}^{\text{far}}\right) \cdot (\Psi_k). \quad (19)$$

The electron density  $n_e$  is calculated in a separate step. It is assumed that  $n_e$  is constant on flux lines, and the density

measurements are mapped onto the poloidal  $\Psi^n$  flux obtained from the preceding iteration step. The section of  $G^{\text{plasma}}$  covering the MSE is derived from equation (2)

$$G^{\text{MSE}} = \left( -\frac{\partial F^{\text{calc,mse}}}{\partial B_R} \mathbf{T}\left(\frac{1}{R^{\text{mse}}} \frac{\partial}{\partial Z}, \mathbf{r}^{\text{mse}}\right) + \frac{\partial F^{\text{calc,mse}}}{\partial B_Z} \right) \times \mathbf{T}\left(\frac{1}{R^{\text{mse}}} \frac{\partial}{\partial R}, \mathbf{r}^{\text{mse}}\right) \cdot (\Psi_k), \quad (20)$$

where  $\mathbf{r}^{\text{mse}}$  are the points of measurements at the intersection of line of sight and neutral beam.

The time for the compilation of the least-squares functional has now effectively been reduced to the time for inverting the Grad–Shafranov operator (12) with Lackner’s method. The CPU time therefore scales with  $N_f * N_g \log N_g$ .

## 5. Application to Tore Supra discharges

The algorithm described above was implemented for Tore Supra, with the geometry of the magnetic sensors and the Faraday chords of the CIEL configuration shown in figure 1. The MSE diagnostic system is presently being build, and therefore not yet incorporated. For the following test cases, we chose the isotropic pressure model. The profiles  $P'$  and  $FF'$  in equation (4) are modelled with polynomials up to second order with vanishing current at the plasma boundary.

A consistency check is the comparison of the magnetic field obtained with the real-time boundary code DPOLO [26]. DPOLO models the vacuum field configuration with a Taylor–Fourier expansion and obtains the plasma boundary in less than a millisecond. As a test case for Tore Supra, we select the Ohmic discharge 28775. EFIT was run using only the data from the magnetic sensors, as in DPOLO. Figure 5 shows a comparison of the isoflux lines for  $t = 5.068$  s and

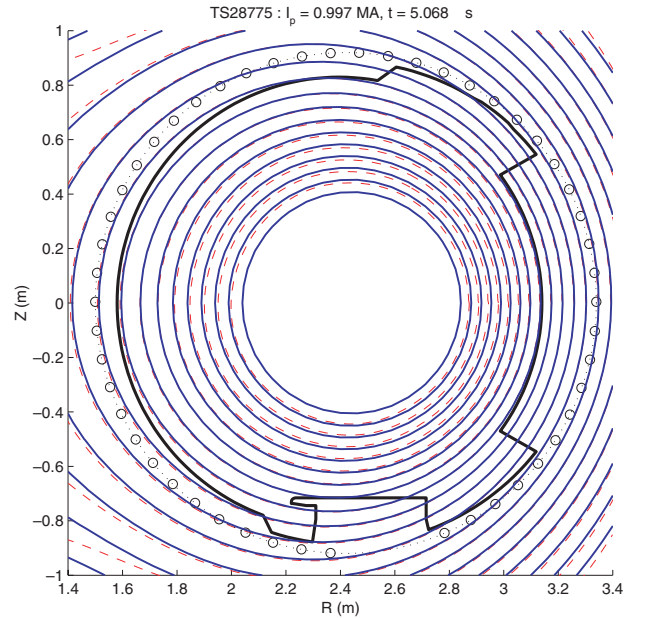


**Figure 5.** Comparison of the EFIT equilibrium reconstruction for Tore Supra discharge 28775 at  $t = 5.068$  s. The solid lines show the isoflux contours of the EFIT reconstruction, the dashed ones those of the reconstruction using the real-time boundary code DPOLO.

demonstrates good agreement in the vicinity of the magnetic sensors down to the plasma boundary. Naturally, the field from DPOLO deviates from the EFIT one inside the plasma, because it does not model the plasma current. Likewise, there are discrepancies far from the boundary, in particular in the corners of the solution domain. Here, EFIT models the field in the vicinity of the poloidal field coils with greater accuracy, whereas the Taylor–Fourier expansion becomes meaningless far away from the plasma boundary.

The accuracy of the fitting algorithm and the approximation by the grid is tested by fitting to a set of exact data produced with a forward solver. As forward solver, EFIT itself is used on a realistic discharge to produce exact artificial data of magnetic sensors, diamagnetic signal, density and Faraday rotation. We choose the high performance discharge 30067, and arbitrarily select a time point at 50 s. A resolution of  $129 \times 129$  is used in the first step to minimize the effect of discretization errors. The obtained data is then fed to the reconstruction algorithm. The same ansatz for  $P'$  and  $FF'$  as in the previous comparison is used. We perform four different reconstructions, using either all data available or omitting Faraday data, each with a grid resolution of  $129 \times 129$  or  $33 \times 33$ . Figure 6(a) shows a comparison of the reference profile with the reconstructed current profiles obtained for the

four different runs. There is almost no noticeable difference, which demonstrates that the discharge is reconstructed very well using exact data. Figure 6(b) shows the deviation of the current profiles in per cent. The deviation for  $129 \times 129$  grid points is below 0.05%, which reflects global errors of the fitting procedure. The deviation for a grid size of  $33 \times 33$  gives an error of about 1%, which is due to discretization errors.

The discharge 30067 is a long pulse with a duration of 220 s. It is therefore well suited to test the CPU time of the code with realistic data. Data from the magnetic sensors and the diamagnetic loop was used for fitting. The individual equilibrium reconstruction for each time slice requires on average 7 iterations. The run was carried out on a 1 GHz Compaq Alpha workstation with a Linpack speed of 1450 MFlops. Table 1 gives a breakdown of average CPU time for one individual step. The first set of runs uses data from the magnetic sensors and the diamagnetic loop, the second set includes also the density data of the 5 vertical chords, and Faraday data from the innermost and outermost vertical chord (see figure 1). All runs are made for the grid sizes of  $33 \times 33$  and  $129 \times 129$  points. No attempt has been made to optimize the post-processing of the results, in particular the calculation of the profiles of safety factor, area and volume Jacobian, etc. Without post-processing, the reconstruction for

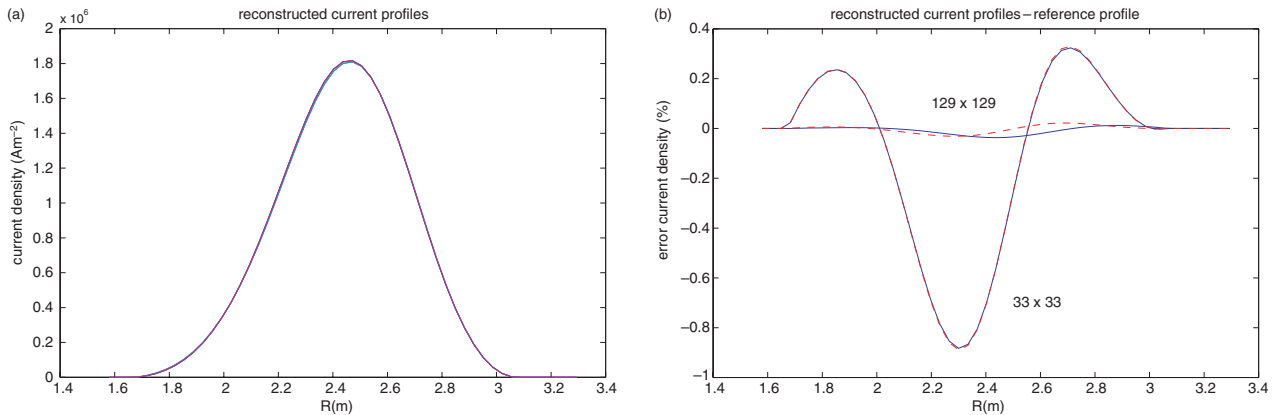


**Figure 6.** Quality of the EFIT reconstruction for exact data. The data was derived from discharge 30067. (a) gives a comparison of reconstructed current profiles with the reference profile of the current density as a function of major radius on the height of the magnetic axis  $J(R, Z = Z_{\text{mag}})$ , showing negligible deviation. (b) shows the difference of reconstructed versus reference profile of the current density in per cent. The flat curves correspond to a resolution of  $129 \times 129$  grid points, the graphs with larger amplitude to  $33 \times 33$  grid points. The graphs with dashed lines mark the comparison with the current profile reconstructed using magnetics data only fit, for both resolutions.

**Table 1.** Average CPU time for a single time step, with a grid size of 33 and 129 radial and vertical points, respectively. The positions marked in italics give the timing for unoptimized parts of the code.

Subtask	CPU time (ms)			
	Magnetics only		Magnetics + Faraday	
	$33 \times 33$	$129 \times 129$	$33 \times 33$	$129 \times 129$
Electron density profile	0	0	7.5	9
Iron model	0.4	4	0.4	4
Compilation of response matrix	3.2	49	9.2	58
Inversion of Grad–Shafranov operator	9.7	195	9.1	187
Least-squares	6.4	7	6.6	7
Location of boundary	2.2	20	2.2	18
<i>Calculation of <math>q</math>, <math>\beta_p</math>, <math>L_i</math> etc</i>	5.3	154	5.3	152
<i>Overhead, I/O etc</i>	5.5	34	11.0	41
Total	32.7	463	51.3	476

a grid size  $33 \times 33$  is carried out in 20 ms for magnetics only, and 35 ms, if Faraday rotation is included in the fit. The addition of Faraday rotation contributes only to the compilation of the response matrix, and the calculation of the density profiles. As expected, the grid size enters mainly in the inversion of the Grad-Shafranov operator, calculation of the response matrix and the tracing of the boundary.

## 6. Conclusions

We have outlined the real-time implementation of an equilibrium reconstruction code based on the EFIT [4] algorithm. For a typical discharge, the code takes roughly 30 ms per time point on a Compaq alpha workstation with a speed of 1450 Linpack MFlops. This compares well with a CPU time of several seconds for the original EFIT code [4]. Further optimization is envisaged. The CPU time of the code scales roughly with the number of grid points  $N_g$  and the number of test functions  $N_f$  for the current profile as  $N_f * N_g \log N_g$ . The code can be easily adapted to the geometry of other machines, like JET or ITER. The time critical routines are based on well-known algorithms, like solving Poisson's equation, sparse matrix multiplication, and bicubic interpolation. Therefore, the code can be easily implemented on other computer platforms, also for parallel environments. On an initial basis, Fortran 95 was selected as programming language. However, it proved useful to convert the coding into matlab, because of the enhanced flexibility and reduced development time. The EFIT algorithm is therefore now available in the matlab language. A reconstruction with EFIT-matlab consumes a few seconds on a personal computer or workstation, and is therefore well suited for interactive applications of selected discharges. The matlab version also allows for easy conversion into other languages, in particular C++ which is the standard language for real-time applications.

The EFIT implementation for Tore Supra requires a model of the iron transformer. It has been demonstrated that it is sufficient for a good reconstruction to model the field of the transformer in the plasma region only. The iron model with 28 fitting variables has been validated with a special dry run. A similar model for the JET device [23] is being optimized. Transformers model for Tokamaks usually have return limbs and are therefore a three-dimensional structure. The iron model (10) can also treat the actual three-dimensional structure and would therefore be a good tool to study error fields generated by the nonaxisymmetry.

The equilibrium reconstruction problem is an inverse problem and requires regularization to guarantee robustness. A reasonable choice is given in definitions (7) and (8). One is left with the task of determining the amount of regularization for the current profile. A generally applicable algorithm for determining these parameters does not seem to be available [30]. For the examples shown in this papers, the parameters were determined by trial and error. A more elaborate method is the *a posteriori* error analysis by calculating a set of equilibria with  $\lambda$  as parameter. The methods of generalized cross-validation [30] or the method of L-curve [16, 31] can be applied to find the optimum regularization. Both techniques are computationally costly and are therefore used only for

advanced analysis of individual discharges. Further work is necessary to develop a faster algorithm to select the regularization automatically or even *a priori*, but this is difficult due to the nonlinearity of the problem (e.g. [32, 33]).

## Acknowledgments

The support of the JET and Tore Supra teams is gratefully acknowledged. The author wishes to thank Drs X. Garbet, M. Ottaviani, E. Joffrin, and J.G. Cordey for their continuous support. I would like to thank F. Saint-Laurent, V. Drozdov and G. Huysmans for helpful discussions.

## References

- [1] Takeda T. and Tokuda S. 1991 *J. Comp. Phys.* **93** 1
- [2] Braams B.J., Gilje W. and Lackner K. 1986 *Nucl. Fusion* **26** 699
- [3] Lao L.L., St. John H., Stambaugh R.D., Kellman A.G. and Pfeiffer W. 1985 *Nucl. Fusion* **25** 1611
- [4] Lao L.L., Ferron J.R., Groebner R.J., Howl W., St. John H., Strait E.J. and Taylor T.S. 1990 *Nucl. Fusion* **30** 1035
- [5] Alladio F. and Crisanti F. 1986 *Nucl. Fusion* **26** 1143
- [6] Blum J., Lazzaro E., O'Rourke J., Keegan B. and Stephan Y. 1990 *Nucl. Fusion* **30** 1475
- [7] Blum J. 1989 *Numerical Simulation and Optimal Control in Plasma Physics* (Paris: Wiley/Gauthier-Villars)
- [8] Hofmann F. and Tonetti G. 1988 *Nucl. Fusion* **28** 1871
- [9] Ferron J.R., Walker M.L., Lao L.L., St John H.E., Humphreys D.A. and Leuer J.A. 1998 *Nucl. Fusion* **38** 1055
- [10] Bosak K. 2001 Real-time numerical identification of plasma in tokamak fusion reactor *Master Thesis* University of Wroclaw, Wroclaw
- [11] Taroni A. and Springmann E. 1986 *JET Report* JET-R(86)03
- [12] Lazzaro E. and Mantica P. 1988 *Plasma Phys. Control. Fusion* **30** 1735
- [13] Wroblewski D. and Lao L.L. 1992 *Rev. Sci. Instrum.* **63** 5140
- [14] Hawkes N.C., Stratton B., Challis C.D., Joffrin E., Rice B., De Angelis R.D. and Zwingmann W. 1999 *EPS Conf. on Control. Fusion and Plasma Physics (Maastricht)* p 277
- [15] Sestero A. and Taroni A. 1976 *Nucl. Fusion* **16** 164
- [16] Zwingmann W., Eriksson L.-G. and Stubberfield P. 2001 *Plasma Phys. Control. Fusion* **43** 1441
- [17] Zwingmann W., Ellis J.J., Lingertat J. and O'Brien D.P. 1993 *Proc. 1993 EPS Conf. on Control. Fusion and Plasma Physics (Lisbon)* p I-195
- [18] Lebedev N.N. 1972 *Special Functions and their Applications* (New York: Dover)
- [19] Press W.H., Teukolsky S.A., Vetterling W.T. and Flannery B.P. 1993 *Numerical Recipes in Fortran 77* (Cambridge: Cambridge University Press)
- [20] Solano E.R., Neilson G.H. and Lao L.L. 1990 *Nucl. Fusion* **30** 1107
- [21] O'Brien D.P., Lao L.L., Solano E.R., Garribba M., Taylor T.S., Cordey J.G. and Ellis J.J. 1992 *Nucl. Fusion* **32** 1351
- [22] Du S. and Wang S. 1995 *Nucl. Fusion* **35** 359
- [23] Zwingmann W., O'Brien D.P. and Bartlett D. 1997 *Proc. 7th Eur. Fusion Theory Conf.* ed Rogister Jülich, p 79
- [24] Trowbridge C.W. 1995 *Finite Elements in Electrical and Magnetic Field Problems* ed M.V.K Chari and P.P. Silvester (New York: Wiley) p 191
- [25] Musolino A., Raugi M. and Visone C. 1995 *IEEE Trans. Magn.* **31** 1706
- [26] Saint-Laurent F. and Martin G. 2001 *Fusion Eng. Des.* **56-57** 761
- [27] Lackner K. 1976 *Comp. Phys. Commun.* **12** 33

- [28] Hockney R.W. and Eastwood J.W. 1988 *Computer Simulation using Particles* (Bristol: Adam Hilger)
- [29] Anderson E. *et al* 1999 *LAPACK Users' Guide* 3rd edn, SIAM, Philadelphia
- [30] Blum J. and Buvat H. 1997 *Large-Scale Optimization with Applications, Part 1: Optimization in Inverse Problems and Design, IMA Volume in Mathematics and its Applications* vol 92 (New York: Springer) p 17
- [31] Hansen P.C. 1994 *Numer. Algorithms* **6** 1
- [32] Gulliksson M., Söderkvist I. and Wedin P.-A. 1997 *SIAM J. Optim.* **7** 208
- [33] Louis A.K. 1995 *Inverse Problems* **11** 1211